Electrical Characteristics of a Modal Filter With a Passive Conductor in the Reference Plane Cutout

Maria Alexandrovna Samoylichenko, Yevgeniy Sergeevich Zhechev, Valerii Pavlovich Kosteletskii, and Talgat Rashitovich Gazizov

***Abstract*—A wider range of operating frequencies, lower supply voltage levels, and increased circuit density of radio-electronic equipment (REE) increase its susceptibility to electromagnetic interferences. Elements of REE are becoming more sensitive to electromagnetic environment especially to ultra-short pulses (USPs) penetrating through front door or back door channels. There is a large variety of noise suppressing devices, but their construction characteristics lead to limited efficiency. Modal filters (MFs), which are based on modal distortion, protect REE from USPs. In this article, the authors present the results of the study of a new method for implementing a MF with a passive conductor in a reference plane cutout and propose two prototypes of the MF with strong and weak couplings. The article presents the results of full-scale and computational experiments in time and frequency domains. For the first time, the decomposition of a USP in the proposed MF configurations is experimentally shown. Besides, we experimentally demonstrated the arrival of additional pulses, the time of which is determined by a linear combination of per-unit-length delays multiplied by the line length. Thus, the proposed approach allows implementing a simple and inexpensive technique for protection against USPs in multilayer printed circuit boards.**

***Index Terms*—Modal filtering (MF), per-unit-length delay, pulse decomposition, quasistatic and electrodynamic simulations, ultra-short pulse (USP).**

I. Introduction

THE INTENSIVE development of radio-electronic equipment (REE), information processing devices that are part of robotic and other systems, and their key importance in various fields, as well as the improvement of the means of intentional electromagnetic exposure, lead to the need for providing proper protection and stable functioning of these devices when they are exposed to electromagnetic interference (EMI). However, the problem is complex, because the disturbances can be arriving through a communications channel (front door) or through the case of the equipment (back door).

Manuscript received May 12, 2020; revised July 1, 2020; accepted July 16, 2020. Date of publication August 4, 2020; date of current version April 14, 2021. This work was supported in part by the Russian Science Foundation under Project No. 19-19-00424 at TUSUR, and in part by the "Impulse" resource sharing center (Russia, Tomsk) with financial support from the Ministry of Science and Higher Education of the Russian Federation under Agreement 075-15-2019-1644, and Project RFMEFI62119X0029. *(Corresponding author: Maria Alexandrovna Samoylichenko.)*

The authors are with the Tomsk State University of Control Systems and Radioelectronics, Tomsk 634050, Russia (e-mail: 1993mary2011@mail.ru; zhechev75@gmail.com; kosteletskiy.vp@gmail.com; talgat@tu.tusur.ru).

Color versions of one or more of the figures in this article are available online at https://ieeexplore.ieee.org.

Digital Object Identifier 10.1109/TEMC.2020.3011407

A common cause of microchip malfunctions is the effect of conducted noise in the form of surge voltages. Ultra-short pulses (USP) are extremely threatening [1]. The main features of their effect are a wide spectral range and a large amplitude. Such a pulse is dangerous due to the high penetration ability attributed to the short exposure time, high power, and wide spectrum.

Pulse surges can result in the malfunctions, such as breakdown of the dielectric layer between conductive elements or p-n junctions of semiconductor components, melting and breaks of current-carrying paths, or destruction of soldering and welding of conductors due to thermo and electrodynamic voltages. Pulsed conductive EMI causes dangerous transients in analog circuits. In digital circuits, they can cause unwanted switching. For critical equipment, including onboard and medical equipment operating in real time, even short-term malfunctions are unacceptable as they can lead to the loss of information, errors in the execution of computational algorithms, loss of control, etc.

There is a large variety of noise-suppressing devices. For example, in work [2], a chip three-terminal multilayer ceramic capacitor EMI filter with a good stopband characteristic has been designed. The structure of the proposed EMI filter presents a new method to improve the stopband characteristics of capacitor EMI filters. In the article [3], it is discussed whether traditional protection concepts provide sufficient protection against at ultra-wideband pulses with significant amplitudes, rise times in the picosecond range, and pulse durations of a few nanoseconds. Furthermore, the possibility of linear filtering is presented with a focus on the protection of high-frequency data lines. The patent [4] shows that some of the results for varistors presented are due only to the packaging and not to the surge protective element in itself. The patent application [5] relates to implantable medical devices and, in particular, to hermetic seal feedthroughs and EMI filters integrated into one or more packages. The invention [6] describes to a passive electronic component architecture employed in conjunction with various dielectrics and combinations of dielectric materials to provide one or more differential and common mode filters for suppressing electromagnetic emissions and surge protection. The invention [7] relates to a multiple contact electrical connector, and in particular to an improved high-speed serial data connector system made up of a modular plug and a receptacle having a polarization slot and a ferrite block filter. The article [8] presents a comprehensive survey of different active EMI filters and their implementations for different power converters presented in the literature. The article

[9] proposes an integrated transmission line common mode and differential mode EMI filter. The article [10] relates to an EMI filter and more particularly to an EMI filter with a differential mode and common mode combination choke that is capable of effectively suppressing EMI. The article [11] presents new measurement system for monitoring the fastest transmission line coupled transients. The article [12] discusses the use of linear filters as protection against UWB pulses and focuses on the implementation of microstrip bandpass filters with very steep edges. In the article [13], the effect of a single-point grounding method of a common-mode EMI filter is first analyzed, and then, in order to eliminate the negative effect of the common ground line, a series-connected grounding method is introduced and analyzed.

However, features of these devices limit the scope of their application. The development of modern protection devices requires that their implementation be simple and cheap; therefore, their improvement is relevant.

It is much simpler in circuit design and manufacturing to use a USP protection device called a modal filter (MF) in which the interference pulse is decomposed in a segment of a coupled line into modes each of which propagates with its own delay so that the MF output pulses have smaller amplitude. For instance, the article [14] presents a new approach to EMC protection through the proper use of inherent properties of coupled interconnects, with some preliminary results of the approach implementation being demonstrated. Particularly, such key characteristics as the difference of per-unit-length modal delays for various types of cables and PCB interconnects have been calculated. It is shown that the difference can be around 1 ns/m, while for special structures, it can be increased up to 5 ns/m. In the article [15], two new simple printed structures are proposed, which provide low-cost and effective protection against ultra-wideband pulses. The first is a structure of asymmetrical MF without resistors, which allows for the 20-time attenuation. The second is another simple structure, a turn of a meander line, allowing for the 2.5-time attenuation. The essential advantages of the MF are its low weight, increased reliability, radiation resistance, and high speed. There have been studied and manufactured different types of MFs, for example, cable MFs for the power supply network [16], mirror-symmetric MFs [17], and MFs with a periodic profile of the coupling region [18].

Previously (above) studied MFs have a passive conductor that takes up space and has mass. Some of them are difficult to manufacture. For example, a mirror-symmetric MF is a three-layer printed circuit board, the implementation of which is difficult, and an MF with a periodic profile complicates the implementation in printed circuit boards. Therefore, it is important to explore new possibilities for implementing the MF. One of the simplest options is obtained by modifying the microstrip line (MSL). The design of such an MF is formed by means of two cutouts in the ordinary plane of the MSL ground, which form a passive conductor between themselves. The results of a numerical simulation of the time response at the MF output are presented in [19], [20], and show that by the weaker coupling between the active and passive conductors, greater attenuation can be achieved. However, no full-scale experiment has been conducted. The purpose of this article is to experimentally confirm that a USP decomposes in an MF with a passive conductor in the cutout of the reference plane with weak and strong couplings.

II. Approaches, Methods, and Designs

This section presents the simulation approaches used in the article, the methods of the experiment, as well as the design characteristics of the proposed MFs.

A. Simulation Approaches

To simulate the time and frequency responses, two approaches were used: quasistatic and electrodynamic.

The quasistatic approach is implemented in the form of fast and accurate mathematical models in the TALGAT system [21]. The system can analyze regular transmission lines with arbitrary cross-sections. A segment of a transmission line with N signal conductors and a reference conductor is described based on a given cross-section. The waveforms of currents and voltages along the line are determined using telegraph equations for the line segment taking into account the boundary conditions. According to the circuit theory, currents and voltages at any point, when only the TEM waves are transmitted, can be related by the following equations:

$$\frac{d}{dx}\mathbf{V} = -\mathbf{ZI} \tag{1}$$

$$\frac{d}{dx}\mathbf{I} = -\mathbf{YI} \tag{2}$$

where $\mathbf{I}$ and $\mathbf{V}$ are matrix columns of size $N \times 1$ of voltages and currents in lines, and

$$\mathbf{Z} = \mathbf{R} + j\omega\mathbf{L} \tag{3}$$

$$\mathbf{Y} = \mathbf{G} + j\omega\mathbf{C} \tag{4}$$

where j is the imaginary unit, ω is the angular frequency, $\mathbf{C}$ is the matrix of per-unit-length coefficients of electrostatic induction of size $N \times N$, $\mathbf{L}$ is the matrix of per-unit-length coefficients of electromagnetic induction of size $N \times N$, $\mathbf{G}$ is the matrix of per-unit-length conductivities of size $N \times N$, and $\mathbf{R}$ is the matrix of per-unit-length resistances of size $N \times N$.

The matrices $\mathbf{L}$ and $\mathbf{C}$ are calculated by the method of moments [22]. The losses in conductors and dielectrics are determined by the matrices $\mathbf{R}$ and $\mathbf{G}$. To calculate the elements of the matrix $\mathbf{G}$, we used the model of the frequency dependence of the relative permittivity and the tangent of the dielectric loss angle of the material FR-4 [23], and the elements of the matrix $\mathbf{R}$ are calculated taking into account the skin effect, proximity effect, and losses in the reference conductor according to the technique [24] implemented in TALGAT. In the simulation, it was taken into account that the increase in segmentation (at the edges of the conductors) results in the increase of accuracy of the results; therefore, in our simulation, we took $n = 5$, where n is the number of segments at the edges of the conductors.

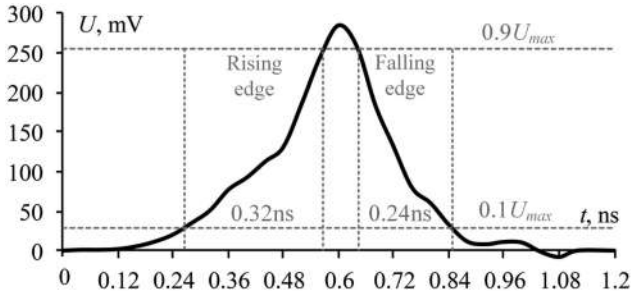

Fig. 1. Digitized signal of the oscilloscope C9-11.

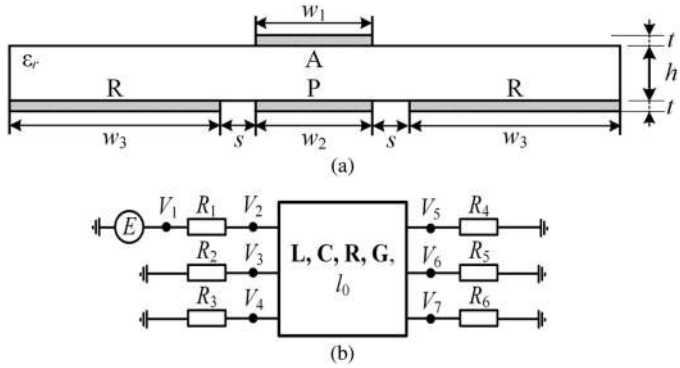

Fig. 2. Cross-section (a) and connection diagram (b) of the MF where the conductors: R—reference, A—active, P—passive.

The electrodynamic approach is well-known and often used in solving problems of electromagnetic compatibility and the propagation of electromagnetic waves. The propagation of electrical signals in transmission media is accurately described by Maxwell's equations. Often, the electrodynamic analysis is implemented by the finite integration method [25], which was used in this article. It provides universal spatial discretization which can be used to solve various kinds of problems. A feature of the finite integration method is that the Maxwell's equations are considered in integral, and not in differential form, like in most numerical methods. To solve these equations, the calculation volume, boundary conditions, and material properties of the device under study are defined. The structure under study was divided into cells with a minimum size of 11.6 μm. In the electrodynamic simulation, as a material for the conductors, we used copper with electrical conductivity $\sigma = 5.8{\cdot}10^7$ S/m.

Running the simulation which uses the two approaches, we selected FR-4 fiberglass as a material of the dielectric substrate. The values of relative permittivity ε_r and dielectric loss tangent tanδ at a frequency of 1 MHz were 4.5 and 0.018, respectively.

The influence of the boundary conditions at the ends of the passive conductor was simulated as follows: "short circuit (SC)–open circuit (OC)," "OC –SC," where the SC was set with a resistance of 10^{-6} Ω, and the OC–10^9 Ω.

In the simulation, we used a digitized signal of an oscilloscope C9-11 measured at a matched load (Fig. 1). The pulse is bell-shaped with the following parameters: the amplitude ($U_{\max}$) is 284 mV, the durations of the rising and falling edges by the levels 0.1–0.9 are 0.32 and 0.22 ns, respectively. The total pulse duration, by the level of 0.5, was 0.18 ns.

B. Modal Filter With a Passive Conductor in the Cutout of the Reference Plane

The main idea of MF is to mitigate an interfering pulse due to the difference in the mode delays of its transverse waves in a multiconductor line. When the pulse propagates in a segment of a line with an inhomogeneous dielectric filling consisting of N conductors (apart from the reference), it can undergo modal distortions until it finally decomposes into N pulses of lower amplitude due to the difference in the specific mode delays in the line. For the complete decomposition of the pulse, the following condition must be met:

$$t_\Sigma < l \min \left| \tau_{i+1} - \tau_i \right|, \quad i = 1, \ldots, \quad N-1 \qquad (5)$$

where t_Σ is the total pulse duration at level 0, l is the length of the segment, and τ_i˜is the linear delay of the ith mode of the segment.

The MF under study is an MSL with two cutouts in the ground plane, between which a passive conductor is formed. Fig. 2(a) shows the cross-section of the MF, where ε_r is the relative permittivity of the substrate, w_1, w_2, and w_3 are the widths of the conductors, t is the thickness of the conductors, h is the thickness of the substrate, and s is the separation of the conductors. As the substrate material, we selected FR-4.

The connection diagram of the MF is shown in Fig. 2(b). The active conductor is connected to a pulse signal source represented on the circuit as an ideal e.m.f. source E and internal resistance R_1. At the other end, the active conductor is connected to the load R_4. The resistance values R_1, R_2, R_4, and R_5 are assumed to be the same and equal to 50 Ω, and for interconnecting the two side (reference) conductors—$R_3 = R_6 = 1$ Ω.

C. MF Layouts

The layouts were made with typical parameters of two-layer foil fiberglass: $t = 35$ μm, $h = 0.18$ mm, $l = 300$ mm. A computational experiment in the time domain has been performed in [19], [20]. With $w_1 = w_2 = w_3 = 1$ mm and $s = 0.5$ mm, when the coupling between the active and passive conductors is weak, it is possible to decrease the amplitude of the USP by about 2.54 times (with resistances at the ends of the passive conductor of 50 Ω) and 4.54 times (with SC–OC at the ends of the passive conductor). And with $w_1 = w_2 = 3.5$ mm, $w_3 = 0.5$ mm, and $s = 3$ mm, when the coupling is strong, the attenuation can be achieved by about five times (with $R = 50$ Ω) and 10 times (with SC–OC). Meanwhile, experimental confirmation of the possibility of such attenuation is of particular interest. Therefore, for conducting a full-scale experiment, MF models with weak and strong couplings between conductors were made. The strengthening of coupling, in this case, is achieved by increasing the width of the active and passive conductors and the distance to the reference conductors. To further simplify the notation, we will refer to the configuration with $w_1 = w_2 = w_3 = 1$ mm, $s = 0.5$ mm as MF1, and to the configuration with $w_1 = w_2 = 3.5$ mm, $w_3 = 0.5$ mm, $s = 3$ mm as MF2.

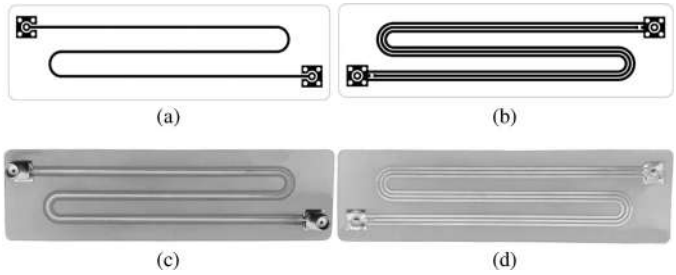

Fig. 3. Photomasks of the MF1 layout: top (a) and bottom (b) layers; photos of the MF1 layout: top (c) and bottom (d) layers.

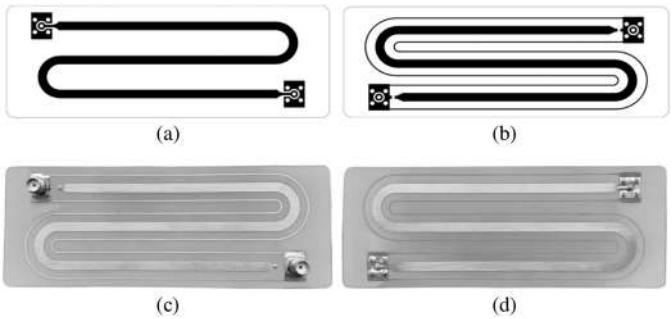

Fig. 4. Photomasks of the MF2 layout: top (a) and bottom (b) layers; photos of the MF2 layout: top (c) and bottom (d) layers.

Next, we performed the tracing of the PCB layouts for MF1 and MF2 configurations. The lengths of the MFs were 300 mm, and the dimensions of the printed circuit boards were 125 mm, so the MFs were made in the form of a meander. To reduce the effect of the turns on each other, we chose an increased distance of $5w$ between them. The layout tracing of MF1 and MF2 is shown in Figs. 3(a), (b) and 4(a), (b). To install SMA connectors, contact pads (CP) are provided with dimensions: 8×8 mm for MF1 and 8×12 for MF2. In each CP, there are five metallized holes with a diameter of 1.2 mm designed to connect conductors on different layers of a PCB. For matching, resistors of standard size 1206 with a resistance of 50 Ω are used. To mount resistors, CPs of 1.7×1.25 mm are installed on the ends of the passive conductors (they are the same for two MFs). The manufactured layouts of MF1 and MF2 are shown in Figs. 3(c), (d) and 4(c), (d).

D. Experimental Study

After manufacturing the MF, geometric parameters were checked. The widths of the printed conductors were verified using a magnifying glass with a measuring ruler [Fig. 5(a)], and the thicknesses of the dielectric substrate and conductors were measured using a mechanical micrometer [Fig. 5(b)]. The real values of geometric parameters were obtained, the average values of which for MF1 were $h = 0.18$ mm, $t = 0.033$ μm, $w_1 = w_2 = w_3 = 1$ mm; and for MF2: $h = 0.18$ mm, $t = 0.033$ μm, $w_1 = w_2 = 3.5$ mm, and $w_3 = 0.5$ mm.

To conduct the experimental study in the time domain, we used a setup whose structural diagram is shown in Fig. 6. For

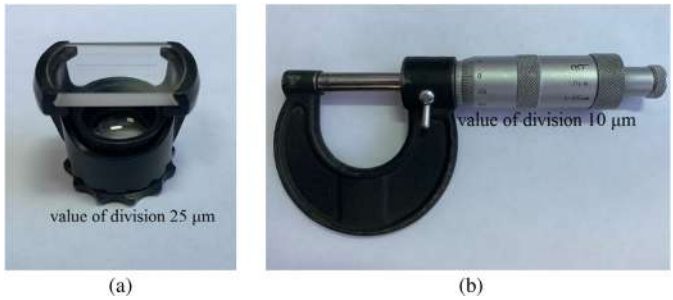

Fig. 5. Magnifying glass with a measuring ruler (a) and a mechanical micrometer (b).

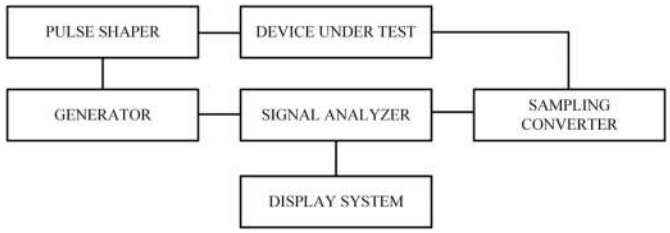

Fig. 6. Experimental setup diagram for the time domain.

Fig. 7. Coaxial adapters used in the experiment.

the required accuracy of signal registration, the horizontal and vertical paths of the measuring system were calibrated. The measurement accuracy of instantaneous values of pulse signals in amplitude is $\pm 3\%$, and time intervals at a given sweep (scan) are $\pm 2\%$.

To connect the MF models with a pulse shaper and a sampling converter, we employed coaxial adapters shown in Fig. 7, namely 3 (PK2-18-01R-03R), 4 (PK2-18-11R-03R), 5 (HYR-1111), and 6 (HYR-1112). When conducting the frequency analysis, adapters 1 (PK2-40-14R-05) and 2 (PK2-50-05-05) were used. The total delay time of the four coaxial transitions (3, 4, 5, and 6) was 230 ps, and the total level of insertion losses did not exceed 1 dB in the frequency range up to 20 GHz.

When conducting experimental studies in the frequency domain, we used a setup whose structural diagram is shown in Fig. 8. The experimental study of the frequency characteristics of the MF was carried out using a P2M-40 transmission and reflection coefficient magnitude meter. Before the measurements, the calibration of channel A (reflection coefficient) and channel B (transmission coefficient) was performed using standard measures. The limiting value of the measurement error was no

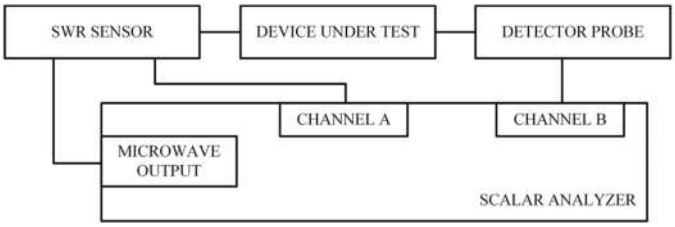

Fig. 8. Experimental setup diagram for the frequency domain.

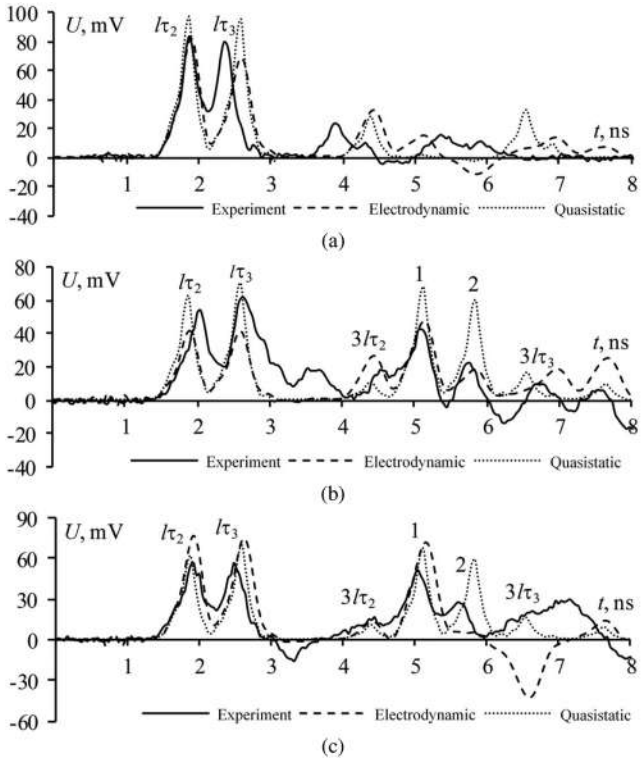

Fig. 9. Voltage waveforms at the output of MF1 obtained for $R_2 = R_5 = 50\,\Omega$ (a), OC–SC (b), and SC–OC (c).

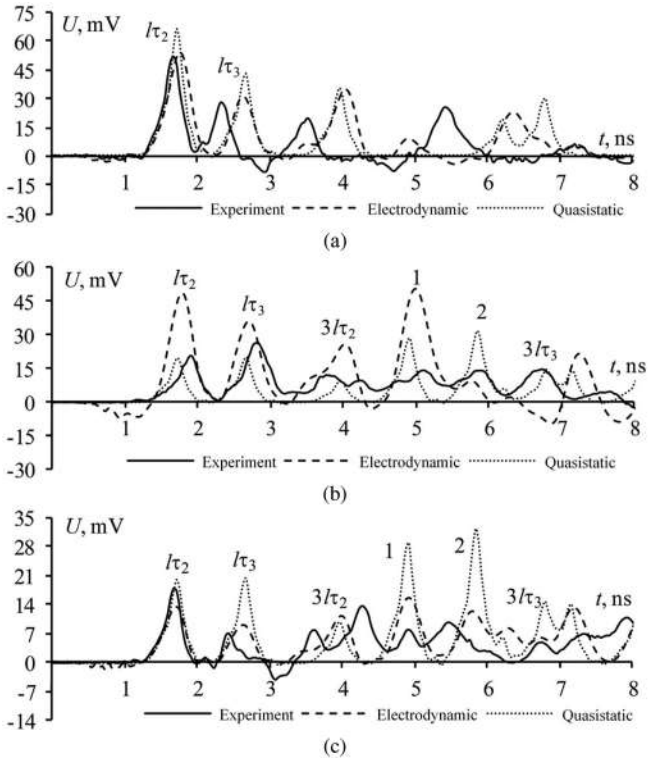

Fig. 10. Voltage waveforms at output of MF2 obtained for $R_2 = R_5 = 50\,\Omega$ (a), OC–SC (b), and SC–OC (c).

TABLE I
AMPLITUDES AND DIFFERENCES OF PER-UNIT-LENGTH DELAYS OF THE FIRST TWO PULSES AT THE OUTPUT OF MF1 OBTAINED WITH VARIOUS TYPES OF ANALYSIS

Para-meters	Quasistatic			Electrodynamic			Experiment		
	50-50	OC-SC	SC-OC	50-50	OC-SC	SC-OC	50-50	OC-SC	SC-OC
U_1, mV	98	58	62	82	41	77	84	54	56
U_2, mV	95	67	67	68	41	75	79	62	52
$\Delta\tau$, ns/m		0.72			0.68			0.54	

TABLE II
AMPLITUDES AND DIFFERENCES OF PER-UNIT-LENGTH DELAYS OF THE FIRST TWO PULSES AT THE OUTPUT OF MF2 OBTAINED WITH VARIOUS TYPES OF ANALYSIS

Para-meters	Quasistatic			Electrodynamic			Experiment		
	50-50	OC-SC	SC-OC	50-50	OC-SC	SC-OC	50-50	OC-SC	SC-OC
U_1, mV	66	20	18	54	48	13	52	20	18
U_2, mV	42	26	20	31	35	8	27	26	7
$\Delta\tau$, ns/m		0.96			0.87			0.8	

more than 1.5 dB in the entire frequency range. Because of the SMA connectors used, the frequency range is limited to 3.5 GHz.

III. RESULTS OF EXPERIMENTAL STUDIES IN THE TIME DOMAIN

Figs. 9 and 10 show the results of field and computational experiments in the time domain for MF1 and MF2, respectively.

Figs. 9 and 10 show that the USP decomposes into two pulses of smaller amplitudes (τ_2 and τ_3). This is explained by the fact that two modes arrive with a difference of about 20 ps; therefore, they overlap. In the experiment, a smaller difference in mode delays is observed. This is because the real ε_r of prototypes under study is less than the value expected in the simulation. The amplitude of the pulses decreases with an increase in the coupling between the conductors and a change in the boundary conditions (OC–SC, SC–OC). The voltage values of the first two pulses during the simulation and the experiment are summarized in Tables I and II. They show that the greatest input exposure attenuation is achieved in MF2 for the SC–OC configuration. The ratio of maximum output voltage to input voltage was 14.2 for quasistatic, 21.84 for electrodynamic, and 15.7 for the experiment. However, from Table II, we can see that MF1 also shows good attenuation.

MF2 demonstrated a large difference in mode delays, as a result of which there is no superposition of pulses. The complete decomposition of a USP can be achieved by increasing the MF length or by choosing a dielectric material with a large ε_r value,

TABLE III
AMPLITUDES OF ADDITIONAL PULSES AT THE OUTPUT OF MF1 OBTAINED WITH VARIOUS TYPES OF ANALYSIS

Parameters	Quasistatic			Electrodynamic			Experiment		
	50-50	OC-SC	SC-OC	50-50	OC-SC	SC-OC	50-50	OC-SC	SC-OC
U_1, mV	-	67	67	-	47	72	-	43	51
U_2, mV	-	59	59	-	18	-	-	22	18

TABLE IV
AMPLITUDES OF ADDITIONAL PULSES AT THE OUTPUT OF MF2 OBTAINED WITH VARIOUS TYPES OF ANALYSIS

Parameters	Quasistatic			Electrodynamic			Experiment		
	50-50	OC-SC	SC-OC	50-50	OC-SC	SC-OC	50-50	OC-SC	SC-OC
U_1, mV	-	28	27	-	47	15	-	10	8
U_2, mV	-	32	28	-	9	12	-	13	10

TABLE V
PER-UNIT-LENGTH MODE DELAYS

	τ_1, ns/m	τ_2, ns/m	τ_3, ns/m
MF1	3.98	4.23	6.58
MF2	3.69	3.73	6.86

TABLE VI
ARRIVAL TIME FOR PULSES OF THREE MAIN MODES

	$\tau_1 l$, ns	$\tau_2 l$, ns	$\tau_3 l$, ns	$3\tau_1 l$, ns	$3\tau_2 l$, ns	$3\tau_3 l$, ns
MF1	1.17	1.24	1.88	3.581	3.81	5.92
MF2	1.11	1.12	2.06	3.32	3.36	6.18

TABLE VII
ARRIVAL TIME FOR ADDITIONAL PULSES (NS)

№	1	2
Combination	$2\tau_2+\tau_3$	$\tau_2+2\tau_3$
MF1	4.51	5.22
MF2	4.30	5.24

as well as by performing parametric optimization according to the corresponding time criteria.

Detailed analysis of Figs. 9 and 10 showed the presence of additional pulses (designated as 1 and 2), which appear when the boundary conditions at the ends of the passive conductor change. As can be seen from Fig. 9(b),(c), the amplitude of the additional pulse 1 is rather large, and 2—small. The analysis of Fig. 10(b),(c) also showed the presence of two additional pulses, but with lower amplitudes. Tables III and IV show the voltage of the additional pulses according to the results of both the simulations and the experiment.

Despite the fact that the shapes of the additional pulses are in good agreement, it is difficult to estimate the exact time of their arrival due to their partial overlap caused by dispersion. To accurately track the dependence of the appearance of additional pulses, the per-unit-length delays, and the arrival times of the three main modes were calculated using quasistatic simulations. The results are shown in Tables V and VI. The resulting combinations and the time of arrival of additional pulses are given in Table VII. According to the results, we can conclude that the delays of additional pulses are determined by the per-unit-length combination of the linear delays of the line modes multiplied by the line length. The appearance of additional pulses in these

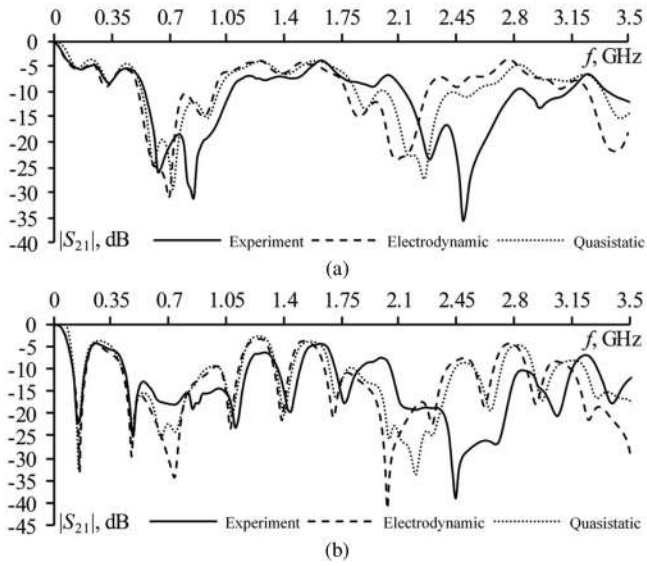

Fig. 11. Frequency dependences of $|S_{21}|$ for MF1 obtained for $R2 = R5 = 50\ \Omega$ (a) and $R2 = 10^{-6}\ \Omega$ and $R5 = 10^{9}\ \Omega$ (b).

configurations is caused by the asymmetry of the cross-sections relative to the reference conductor and the asymmetry of the boundary conditions. This leads to the arrival of waves with different propagation velocities in opposite directions. In the 50-50 configuration, due to better alignment, the additional pulses are not so well pronounced.

Thus, the experimental results confirm the possibility for the initial pulse to decompose at the end of the active conductor into a sequence of pulses of lower amplitudes. It is shown that with the increase of the coupling and changes in the boundary conditions, it is possible to achieve a greater decrease of the USP level. However, there appear additional pulses, the delays of which are determined by a linear combination of the per-unit-length delays of the line modes multiplied by the line length. The results of field and computational experiments are in good agreement in the waveform and arrival time. The deviation of the simulation results from experimental results is caused by the fact that the influence of coaxial microstrip and coaxial transitions, as well as the difference in the electrical characteristics of the dielectric, were not taken into account.

IV. RESULTS OF EXPERIMENTAL STUDIES IN THE FREQUENCY DOMAIN

Figs. 11 and 12 show the results of the experiment and simulation of the frequency dependence of $|S_{21}|$ for MF1 and MF2. It should be noted that the devices under study are bidirectional; therefore, the results are given only for options 50-50 Ω and OC–SC.

According to the results of field and computational experiments in the frequency domain, we can conclude that the structures under study can be referred to as low-pass filters. The cutoff frequencies (-3 dB) and resonant frequencies for them are summarized in Table VIII.

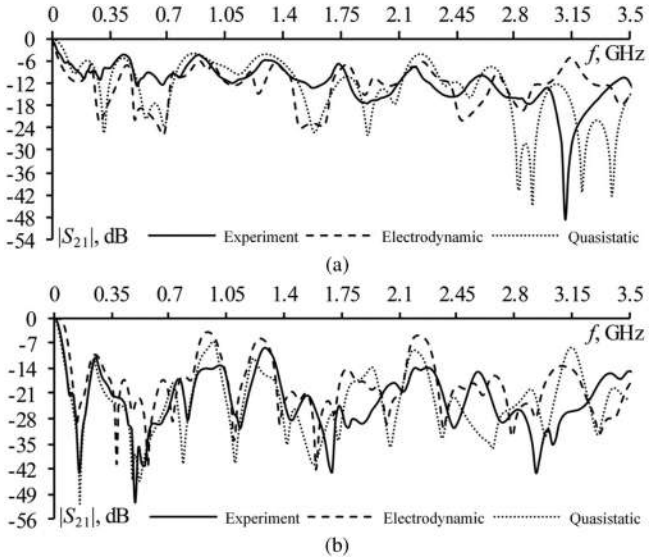

Fig. 12. Frequency dependences of $|S_{21}|$ for MF2 obtained for $R2 = R5 = 50\ \Omega$ (a) and $R2 = 10^{-6}\ \Omega$ and $R5 = 10^{9}\ \Omega$ (b).

TABLE VIII
CUTOFF FREQUENCIES AND RESONANCE FREQUENCIES FOR MF1 AND MF2

Frequency, MHz	Quasistatic		Electrodynamic		Experiment	
	50-50	OC-SC	50-50	OC-SC	50-50	OC-SC
f_{cMF1}	61	73	90	100	69	89
f_{cMF2}	20	27	77	81	24	27.5
f_{r1MF1}	-	156	601	160	629	149
f_{r2MF1}	696	471	720	480	849	489
f_{r1MF2}	291	156	320	150	289	149
f_{r2MF2}	676	476	690	390	669	489

The band-pass of MFs with the weak coupling is greater than with the strong one. Changing the boundary conditions at the ends of the passive conductor allows increasing the band-pass. According to the results of the experimental study, the largest band-pass is 89 MHz for MF1 with OC–SC. Table VIII shows that in the configuration of the OC–SC, the frequencies of the first and second resonances decrease. Thus, the results of field and computational experiments are in good agreement. The dissimilarity in the results originates from the different values of electrical parameters of real prototypes and their mathematical models. For example, the values of ε_r and $\tan\delta$ may be different, which shifts the diagrams by frequency. In addition, the influence of coaxial microstrip and coaxial transitions, which introduce frequency-dependent losses, was not taken into account in the simulation. The difference between the results of quasistatic and electrodynamic simulations, however, results from the limitations of the approaches and methods used.

In terms of low-pass filtering, the configuration of SC–OC in MF1 and MF2 is more preferable. The presence of pronounced resonances in the mismatched configuration allows increasing the insertion loss. It should be noted that MF1 and MF2 have a sufficiently wide suppression band, which is relevant for suppressing wideband conductive interference.

V. CONCLUSION

This article considers the protection of EE from the effects of conducted noise of short duration by means of MF technology. The experimental study was conducted in the time and frequency domains. To confirm the results obtained, we performed simulation by two different approaches, in which the measured parameters of the cross-sections of each MF were taken into account, and then, the results of the simulations and experiment were compared. As the excitation, we used a digitized waveform of a real USP from the generator output.

It was experimentally proven that a USP could successfully decompose in the MF with a passive conductor implemented in the cutout of the reference plane. It is shown that an increase in the coupling between the active and passive conductors, as well as a change in the boundary conditions at the ends of the passive conductor, allow for a greater attenuation of the USP. When conducting a full-scale experiment, the maximum decrease of the USP amplitude was achieved 15.5 times. The experiment also showed the presence of additional pulses, which appear when the boundary conditions at the ends of the passive conductor change, and their delays are determined by a linear combination of the per-unit-length delays of the line modes multiplied by the line length. It was revealed that the configuration with weakly coupled MFs has a larger band-pass. Changing the boundary conditions at the ends of the passive conductor allows increasing the band-pass. According to the results of the experimental study, the largest band-pass is 89 MHz for the MF with weak coupling at OC–SC. In the OC–SC configuration, the frequencies of the first and second resonances are reduced for both devices. The results of field and computational experiments in the time and frequency domains are in good agreement. The deviation of the simulation results from experimental results is caused by the fact that the influence of coaxial microstrip and coaxial transitions, as well as the difference in the electrical characteristics of the dielectric, were not taken into account.

Research and development of interference suppression devices based on MF, including MFs with a passive conductor in the cutout of the reference plane, proved to be promising. The results of this article will be useful in the design of such devices.

ACKNOWLEDGMENT

The authors sincerely appreciate all valuable comments and suggestions from the reviewers, which helped us to improve the quality of the article.

REFERENCES

[1] Z. M. Gizatullin and R. M. Gizatullin, "Investigation of the immunity of computer equipment to the power-line electromagnetic interference," *J. Commun. Technol. Electron.*, vol. 61, no. 5, pp. 546–550, 2016.
[2] X.-C. Wang, Y.-Y. Sun, J.-H. Zhu, Y.-H. Lou, and W.-Z. Lu, "Folded feedthrough multilayer ceramic capacitor EMI filter," *IEEE Trans. Electromagn. Compat.*, vol. 59, no. 3, pp. 996–999, Jun. 2017.
[3] T. Weber, R. Krzikalla, and L. Haseborg, "Linear and nonlinear filters suppressing UWB pulses," *IEEE Trans. Electromagn. Compat.*, vol. 46, no. 3, pp. 423–430, Aug. 2004.
[4] D. Mansson and R. Thottappillil, "Comments on linear and nonlinear filters suppressing UWB pulses," *IEEE Trans. Electromagn. Compat.*, vol. 47, no. 3, pp. 671–672, Aug. 2005.

[5] N. A. Youker, L. D. Swanson, J. E. Hansen, and W. J. Linder, "Integrated electromagnetic interference filters and feedthroughs," U.S. Patent 7 719 854 B2, May 2010.
[6] A. A. Anthony, "Paired multi-layered dielectric independent passive component architecture resulting in differential and common mode filtering with surge protection in one integrated package," U.S. Patent 6 873 513 B2, Mar. 2005.
[7] K. S. Boutros, R. Pike, and M. D. Dima, "Modular plug connector and improved receptacle therefore," U.S. Patent 6 276 943, Aug. 21, 2001.
[8] B. Narayanasamy and F. Luo, "A survey of active EMI filters for conducted EMI noise reduction in power electronic converters," *IEEE Trans. Electromagn. Compat.*, vol. 61, no. 6, pp. 2040–2049, Dec. 2019.
[9] L. Zhao, R. Chen, and J. Van Wyk, "An integrated common mode and differential mode transmission line RF-EMI filter," in *Proc. IEEE 35th Annu. Power Electron. Specialists Conf.*, 2004, pp. 4522–4526.
[10] H. Y. Ho, "Electromagnetic interference filter," U.S. Patent 8 098 495, Jan. 17, 2012.
[11] T. Weber and J. L. Ter Haseborg, "Hardening of electronics against transmission line coupled UWB – Signals," in *Proc. XXVIIth URSI General Assem.*, vol. 27, 2002, pp. 1–4.
[12] R. Krzikalla, T. Weber, and J. Ter Haseborg, "Interdigital microstrip filters as protection devices against ultrawideband pulses," in *Proc. IEEE Int. Symp. Electromagn. Compat.*, vol. 2, 2003, pp. 1313–1316.
[13] H. Chen, "Series-connected grounding of common-mode EMI filter," *IEEE Trans. Electromagn. Compat.*, vol. 52, no. 4, pp. 1066–1068, Nov. 2010.
[14] T. R. Gazizov and A. M. Zabolotsky, "New approach to EMC protection," in *Proc. 18th Int. Zurich Symp. Electromagn. Compat.*, 2007, pp. 273–276.
[15] A. T. Gazizov, A. M. Zabolotsky, and O. A. Gazizova, "New printed structures for protection against UWB pulses," in *Proc. 16th Int. Conf. Young Specialists Micro/Nanotechnol. Electron Devices*, 2015, pp. 120–122.
[16] T. R. Gazizov and A. M. Zabolotsky, "Experimental results on UWB pulse propagation in low voltage power cables with different cross sections," *IEEE Trans. Electromagn. Compat.*, vol. 54, no. 1, pp. 229–231, Feb. 2012.
[17] E. B. Chernikova, A. O. Belousov, and A. M. Zabolotsky, "Comparative analysis of microstrip and reflection symmetric four-conductor modal filters," in *Proc. Int. Siberian Conf. Control Commun.*, 2019, pp. 1–4.
[18] R.R. Khazhibekov, A. M. Zabolotsky, and M. V. Khramtsov, "Study of the characteristics of a modal filter with different periodic profiles of the coupling region," in *Proc. Int. Multi-Conf. Eng. Comput. Inf. Sci.*, 2017, pp. 506–509.
[19] M. A. Samoylichenko and T. R. Gazizov, "Simulation of broad-side coupled modal filter with passive conductor in reference plane cutout," in *Proc. IOP Conf. Ser.: Mater. Sci. Eng.*, vol. 560, 2019, Art. no. 012040.
[20] M. A. Samoylichenko, "Influence of boundary conditions and coupling enhancement on the attenuation of a modal filter with a passive conductor in the reference plane cutout," in *Proc. IEEE Int. Multi-Conf. Eng. Comput. Inf. Sci.*, 2019, pp. 0237–0240.
[21] S. P. Kuksenko, "Preliminary results of TUSUR University project for design of spacecraft power distribution network: EMC simulation," in *Proc. IOP Conf. Ser.: Mater. Sci. Eng.*, vol. 560, 2019, Art. no. 012110.
[22] T. R. Gazizov, "Analytic expressions for mom calculation of capacitance matrix of two dimensional system of conductors and dielectrics having arbitrary oriented boundaries," in *Proc. IEEE EMC Int. Symp. Rec. Int. Symp. Electromagn. Compat.*, 2001, pp. 151–155.
[23] A. R. Djordjevich, R. M. Biljie, V. D. Likar-Smiljanic, and T. K. Sarkar, "Wideband frequency-domain characterization of FR-4 and time-domain causality," *IEEE Trans. Electromagn. Compat.*, vol. 43, no. 4, pp. 662–667, Nov. 2001.
[24] G. Matthaei and G. Chinn, "Approximate calculation of the high-frequency resistance matrix for multiple coupled lines," in *Proc. IEEE MTT-S Microw. Symp. Dig.*, 1992, pp. 1353–1354.
[25] M. Clemens and T. Weiland, "Discrete electromagnetism with the finite integration technique," *Prog. Electromagn. Res.*, vol. 32, pp. 65–87, 2001.

Maria Alexandrovna Samoylichenko received the B.Sc. and M.Sc. degrees in engineering from Tomsk State University of Control Systems and Radioelectronics (TUSUR), Tomsk, Russia, in 2015 and 2017, respectively.

She is currently a Postgraduate Student and works as an Engineer with TUSUR. She has authored and coauthored 13 scientific papers.

Yevgeniy Sergeevich Zhechev received the B.Sc. and M.Sc. degrees in engineering from Tomsk State University of Control Systems and Radioelectronics (TUSUR), Tomsk, Russia, in 2016 and 2018, respectively.

He is currently a Postgraduate Student and also works as a Junior Researcher with TUSUR. He has authored 22 scientific papers.

Valerii Pavlovich Kosteletskii received the B.Sc. and M.Sc. degrees in engineering from Tomsk State University of Control Systems and Radioelectronics (TUSUR), Tomsk, Russia, in 2015 and 2017, respectively.

He is currently a Postgraduate Student and also works as a Junior Researcher with TUSUR. He has authored 11 scientific papers.

Talgat Rashitovich Gazizov was born in 1963. He received the Ph.D. degree in improvement of circuit board interconnections and the D.Sc. degree in reduction of electric signal distortion in the interconnections and effects of power electromagnetic interference from Tomsk State University of Control Systems and Radioelectronics, Tomsk, Russia, in 1999, and 2010, respectively.

He has authored/coauthored more than 360 scientific papers, including 11 books. His research interest includes signal integrity problem.